International Journal of Nanoscience, Vol. 1, Nos. 3 & 4 (2002) 337–346


# ATOMISTIC CAPACITANCE OF A NANOTUBE ELECTROMECHANICAL DEVICE

SLAVA V. ROTKIN*,§, VAISHALI SHRIVASTAVA†,
KIRILL A. BULASHEVICH‡, and N. R. ALURU*,†

*Beckman Institute, UIUC, 405 N. Mathews, Urbana, IL 61801, USA
†General Engineering Department, UIUC, 104 S. Mathew
Urbana, IL 61801, USA
‡Ioffe Institute, 26 Politekhnicheskaya st., St. Petersburg 194021, Russia
§rotkin@uiuc.edu

Received 1 September 2002
Revised 26 September 2002

An atomistic capacitance is derived for a single-wall carbon nanotube in a nanoelectromechanical device. Multi-scale calculation is performed using a continuum model for the geometrical capacitance, and statistical and quantum mechanical approaches for the quantum capacitance of the nanotube. The geometrical part of the capacitance is studied in detail using full three-dimensional electrostatics. Results reported in this paper are useful for compact modeling of the electronic and electromechanical nanotube devices.

*Keywords*: Nanotube; quantum capacitance; theory; electronic structure.

## 1. Introduction

Carbon nanotubes are promising for electronic[1] and electromechanical[2,3] devices as these natural nanoscale objects have diameters ∼1–50 nm, high mechanical stability and interesting electronic properties. Metallic nanotubes, degeneratively doped and intrinsic semiconductor nanotubes were observed experimentally.[4] Electronic structure fundamentals of an ideal single-wall nanotube (SWNT) were understood in detail but no known device theories exist. The development of device theories for carbon nanotubes and further progress in their technology can make the carbon-based materials as attractive as standard semiconductor materials.

We recently addressed electrostatics of nanotubes[5–7] at different levels of accuracy. First, a general macroscopic approach has been employed to model the nanotube response in a nanoelectromechanical system (NEMS),[5] which gives a good estimate for an electrostatic force for a large diameter multiwall nanotube. When a voltage is applied between the nanotube and a backgate, the charge is accumulated on the tube surface. We improved the understanding of the microscopics of the charge accumulation on the single-wall nanotube within a continuum statistical model[6] and a quantum mechanical approach.[7] One needs to use the quantum

mechanical calculation for the electrostatic force in a narrow nanotube NEMS because of a high depolarization of the external potential by the valence electrons of the tube. A simple description has been proposed in Ref. 6 as an alternative to a full quantum mechanical calculation of the electrostatics. In the proposed approach an atomistic capacitance of the nanotube is computed as the sum of two terms: the quantum capacitance[6,8] and the geometric capacitance. The latter is a full analogue of a macroscopic capacitance of a metallic cylinder of the same shape as the nanotube. However, in our earlier papers this geometric or classical capacitance has been approximated by the well known capacitance of an infinite metal wire.[9]

In this article we study the region of applicability of classical approximation for a finite tube by solving the Poisson equation in the finite geometry of a NEMS device. We show how the device geometry influences the geometrical capacitance.

## 2. Atomistic Capacitance of a SWNT

We studied two types of SWNT device designs. The first design comprises a straight nanotube fixed (suspended without a slack) between two metal side electrodes over a backgate electrode. This is referred to as a "string" NEMS design. The side electrodes are kept at the same potential with respect to the backgate. This design is standard for semiconductor microelectromechanical systems. A first experimental realization of a single SWNT string NEMS appeared recently.[3] The second design is a "cantilever" NEMS device whose geometry is shown in Fig. 1. The cantilever nanotube electromechanical switch has been theoretically studied in Ref. 5. The same geometry can be used to simulate the behavior of the nanotube nanotweezers (for experimental data see Ref. 2), because the electrostatic potential for the cantilever geometry is the same as for the symmetrical nanotweezers.[9]

In order to calculate the charge distribution of the SWNT as a function of the total (acting) potential we represent the potential as a sum of the external and induced potentials:

$$\phi^{\mathrm{act}} = \phi^{\mathrm{xt}} + \phi^{\mathrm{ind}} \,. \tag{1}$$

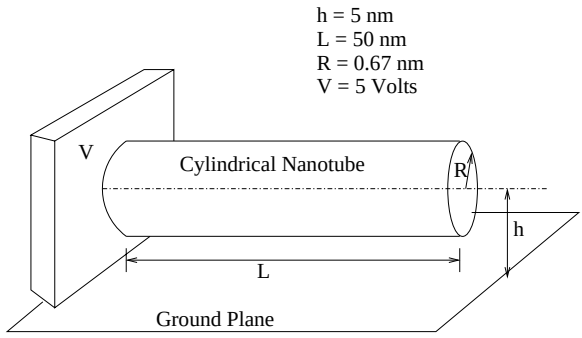


Fig. 1. Geometry of a cantilever device. The radius of the simulated nanotube is 0.67 nm and its length is 50 nm. The gap between the axis of the nanotube and the ground plane is 5 nm.

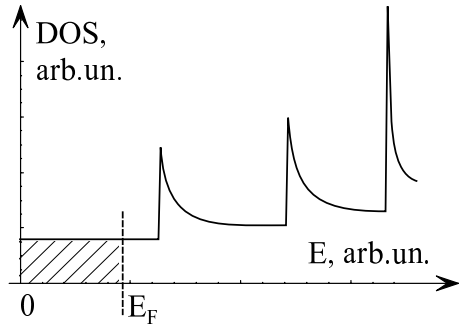


Fig. 2. Density of states of the metallic SWNT near the Fermi level: shaded area represents an extra charge induced in the SWNT by shifting the Fermi level away from the charge neutrality level.

The statistical model assumes that the induced charge is an integral over the nanotube density of states (DOS) from a local charge neutrality level to a local chemical potential which becomes Fermi level at zero temperature (see Fig. 2). The local chemical potential is supposed to follow the local acting potential. Great simplification is achieved in case of a metallic nanotube operating at low voltage when the Fermi level shifts within the first subband. Then, the electron dispersion is linear and the DOS is constant and equals $\nu_M = 8/(3b\gamma)$. Here $b \simeq 1.4$ Å is the interatomic distance and $\gamma \simeq 2.7$ eV is the hopping integral (we use standard definitions for TBA calculation of DOS). Within this approximation of the linear energy dispersion in the lowest subband, the induced charge density reads as:

$$\rho(z) = -e^2 \nu_M \phi^{\mathrm{act}}(z)\,. \tag{2}$$

We note that Eq. (2) holds in one-dimensional (1D) case; while in 2D the charge density is proportional to the electric field (first derivative of the potential) and in 3D the charge density is proportional to the Laplacian of the potential (the Poisson equation).

In order to obtain a selfconsistent solution for the charge density one has to calculate the induced potential. With the use of a Green's function, $G(\mathbf{r}, \mathbf{r}')$, it reads as:

$$\phi^{\mathrm{ind}}(\mathbf{r}) = 4\pi \int G(\mathbf{r}, \mathbf{r}')\rho(\mathbf{r}')\mathbf{dr}'\,. \tag{3}$$

The Green's function of a 1D system is known to diverge logarithmically until some external screening is considered. In case of a nanotube device, this screening is due to the closest gates/contacts. An equation, giving the nanotube charge density implicitly, follows from Eqs. (2) and (3) and reads as:

$$-\frac{\rho(\mathbf{r})}{e^2\nu_M} - 4\pi \int G(\mathbf{r}, \mathbf{r}')\rho(\mathbf{r}')\mathbf{dr}' = \phi^{\mathrm{xt}}(\mathbf{r})\,. \tag{4}$$

The equation can be inverted analytically in simple cases. In general, it allows only numerical solution or may be expressed as a series.

We found that the nanotube may be divided into three parts: two contact regions and a "central" region.[6] The side parts are the regions near the contacts and are of length about several $h$, where $h$ is the distance to the gate. Aspect ratio of devices of the state-of-art nanotube technology is very high, which means that the length of the nanotube, $L$, is much larger than $h$. Then, the central region of the nanotube covers almost the entire device length.

The electrostatics of the central region is elementary and allows an analytical solution for Eq. (4). Because of the screening of the Coulomb interaction by the backgate electrons and the valence electrons of the nanotube, the corresponding Green's function is short-ranged. Therefore, at a distance of about 2–3$h$ from the contact, the selfconsistent charge density is given by a simple expression:

$$\rho \simeq \rho_\infty = -\frac{\phi^{\mathrm{xt}}}{C_g^{-1} + C_Q^{-1}} \simeq -\phi^{\mathrm{xt}} C_g \left(1 - \frac{C_g}{C_Q}\right), \tag{5}$$

here we used notations $C_g^{-1} = 2\log(2h/R)$ and $C_Q^{-1} = 1/(e^2\nu_M)$ for the inverse capacitance (potential coefficient) of a straight metal cylinder and the atomistic correction, respectively. $\rho_\infty$ stands for an equilibrium charge density of the SWNT, calculated at a distance from the side electrode much larger than the distance to the backgate, $h$. We will extend this calculation in the next section to take into account the finite size effects for the $C_g$.

## 3. Full Electrostatics Calculation of the Geometric Capacitance

### 3.1. *The model and method*

In this section we present a full electrostatic capacitance calculation which is based on the following governing equation:

$$\bigtriangledown^2 \phi = 0 \qquad \mathbf{r} \in \bar{\Omega} \tag{6}$$

along with appropriate boundary conditions for the exterior electrostatic problem in 3D as given by[10]:

$$\phi = g_1 \qquad \text{on} \quad d\Omega_1 \tag{7}$$

and

$$\phi = g_2 \qquad \text{on} \quad d\Omega_2\,, \tag{8}$$

where $d\Omega_1$ ($d\Omega_2$) denotes the surface or boundary of a conductor 1 (2), and $\bar{\Omega}$ is the domain exterior to the conductors 1 and 2. A potential of $g_1$ ($g_2$) is applied to the conductor 1 (2). The objective is to compute the surface charge density on the two conductors.

Boundary element method[11] is an efficient technique to solve the exterior electrostatic problem. The boundary integral equation for the electrostatic problem in 3D is given by:

$$\phi(P) = \int_{d\Omega} G(P,Q)\sigma(Q)d\Gamma_Q\,, \tag{9}$$

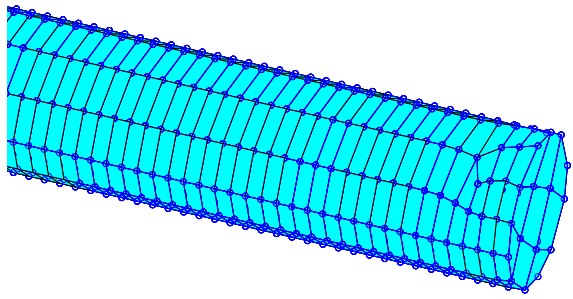

Fig. 3. Discretized nanotube of length 50 nm and radius 0.67 nm. A magnified view of the free end of the cantilever nanotube is shown. Typical length of discretization is 0.03 nm.

where $\sigma$ is the unknown surface charge density, $P$ is the source point, $Q$ is the field point, $G$ is the Green's function and $d\Omega = d\Omega_1 \cup d\Omega_2$. In three dimensions,

$$G(P,Q) = \frac{1}{4\pi\varepsilon|P-Q|}\,, \tag{10}$$

where $|P-Q|$ is the distance between the source point $P$ and the field point $Q$ and $\varepsilon$ is the permittivity of the medium.

In the classical boundary element method, the surface of the conductors is discretized into panels as shown in Fig. 3. The surface charge density is interpolated using bilinear shape functions.[10] The boundary integral equation (9) for a source point $P$ can be rewritten as:

$$\phi(P) = \sum_{k=1}^{NE} \int_{d\Omega_k} \frac{1}{4\pi\varepsilon|P-Q_k|}\sigma_k d\Gamma_{Q_k}\,, \tag{11}$$

where $NE$ is the number of panels, $d\Omega_k$ is the surface of the $k$th panel, $Q_k$ is the field point on the $k$th panel and $\sigma_k$ is the unknown charge density on the $k$th panel. Depending on the location of the source point $P$ and the field point $Q$ various techniques are used to evaluate the integrand in Eq. (11). When $P$ and $Q$ are in the same panel the integration is performed analytically and when $P$ and $Q$ are in different panels the integration is performed numerically (see Ref. 10 for details). Equation (11) can be rewritten in a matrix form as:

$$\mathbf{A}\bar{\sigma} = \bar{\phi}\,, \tag{12}$$

where $\mathbf{A}$ is an $NP \times NP$ coefficient matrix, $\bar{\phi}$ is a right hand side $NP \times 1$ vector, $\bar{\sigma}$ is an unknown $NP \times 1$ vector, and $NP$ is the number of nodes on the surface of the conductors. The entries of the coefficient matrix are given by:

$$A(i,j) = \int_{d\Omega_j} \frac{1}{4\pi\varepsilon|P_i - Q_j|} d\Gamma_{Q_j} \qquad i,\, j = 1,\ldots,NP\,. \tag{13}$$

The $\bar{\phi}$ vector in Eq. (12) is the given potential boundary condition. The unknown charge density vector can be computed by solving the matrix problem in Eq. (12).

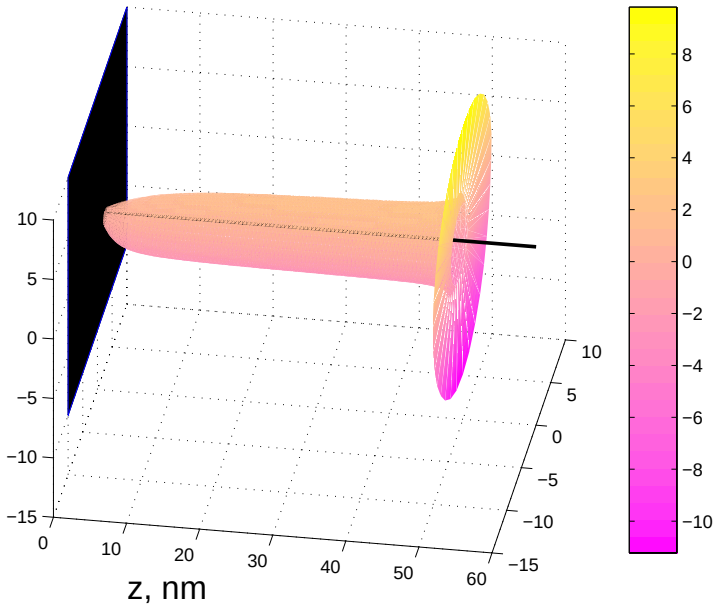


Fig. 4. 3D plot of the surface charge density distribution on a cantilever nanotube of radius 0.67 nm, length 50 nm and the distance from the ground plane 5 nm.

We plot a typical solution of the problem as a color map in Fig. 4. The electron density is shown as a vector normal to the nanotube axis. The closer the point of the surface to the axis, the smaller the charge density. In the vicinity of the side contact (shown as a black plane), the charge density is smaller. At the free end of the tube, it increases. The color map shows that the charge density is not uniform along the equator in contrast to the one-dimensional wire model.

Once the charge density $\bar{\sigma}$ is known the capacitance of the conductor with applied potential $g_1$ can be computed using,[12]

$$C_g = \frac{1}{g_1} \int_{d\Omega_1} \sigma(Q) d\Gamma_Q \,. \tag{14}$$

The results of this calculation are presented below.

### 3.2. *Results and discussion*

The capacitance of an infinite wire is logarithmic in nature and can be computed as the product of length of the tube and specific capacitance: $C_\infty = 1/2 \log(2h/R)$. The capacitance of a metal cylinder of finite length connected to the metal side contact(s) from one (both) end(s) is smaller than $L \times C_\infty$, the capacitance within the infinite wire approximation for the same length. The reasons are two-fold: first, the contact region is depleted as the external potential is screened by the free electrons in the contact. Second, the charge distribution is nonuniform along the length of the tube because of closed (free and/or attached to the metal surface)

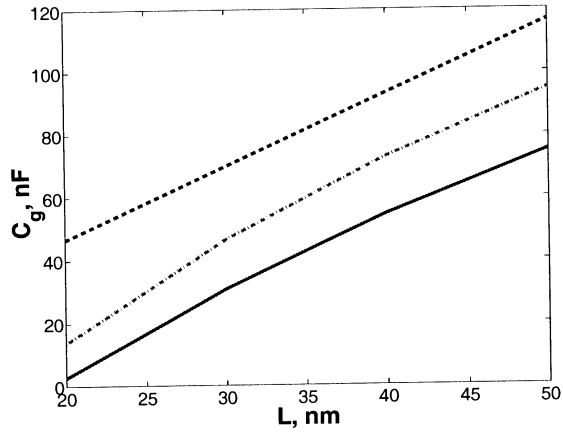


Fig. 5. Dependence of the capacitance of the nanotube of radius 0.67 nm on the length of the NEMS, $L$. The capacitance of the string device is shown as a full line and the capacitance of the cantilever device is shown as a dot–dashed line. The specific capacitance of the infinite wire times the length is plotted as a dashed line.

ends of the tube, i.e., finite size effect. We studied the finite size effect by changing the actual length of the simulated NEMS device, $L$. The results are presented in Fig. 5. Both string and cantilever devices have capacitance which differs from the limit of the infinite wire model. However, this difference decreases with the length of the device.

The effect of the side contact screening has been studied by calculating the dependence of the capacitance on the distance to the ground plane (NEMS backgate), $h$, for a fixed length of the device. In this case, we expect that with the increase in

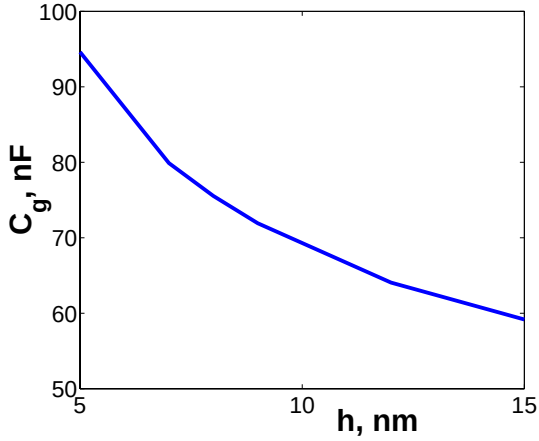


Fig. 6. Dependence of the capacitance of the cantilever nanotube of radius 0.67 nm on the gap between the nanotube and the ground plane (backgate of the device), $h$.

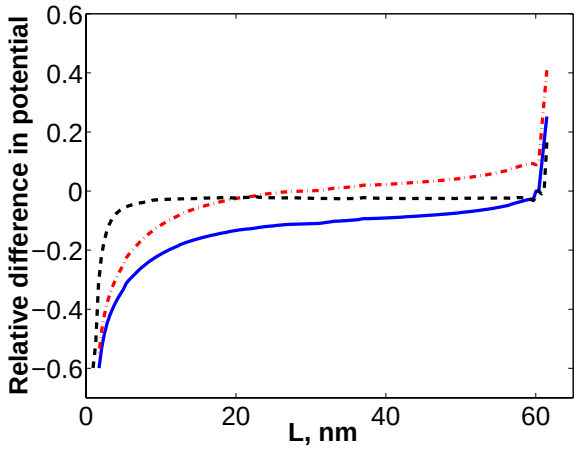


Fig. 7. The comparison of results of the full electrostatics calculation and the one-dimensional model. The relative difference of the calculated electrostatic potentials $((\phi_{3D} - \phi_{1D})/\phi_{3D})$ is shown for the lowest part of the tube (—), for the central line of the tube (- · - · -) and for the uppermost part of the tube (- - -). The difference at the central line is due to the finite size effects. The potential difference between top and bottom of the tube shows the transverse polarization of the metal cylinder which is not taken into account by the 1D wire approximation.

the distance of the nanotube to the gate the screened area of the nanotube surface grows, and the change in the capacitance becomes more prominent. As we have discussed above, the screening diminishes the NEMS capacitance, and therefore, the geometric capacitance decreases with $h$. We plot the cantilever NEMS capacitance in Fig. 6. The string NEMS has the same behavior (not shown).

The effects of the screening and the finite size result in a distribution of the charge along the nanotube which is different from what we obtained in the infinite wire approximation. These two results are compared in Fig. 7.

## 4. Quantum Mechanical Calculation of the Quantum Capacitance

We derived the Green's functions for several realistic device geometries and calculated the selfconsistent charge densities in the last section. These charge densities were compared with the results of the quantum mechanical computation. We solved the Schrödinger and Poisson equations for the valence pi-electrons of a metallic armchair [10, 10] SWNT in one subband approximation (in full neglecting the intersubband or sigma–pi mixing which has been estimated and is of minor importance for our problem). The statistical, semiclassical and full quantum mechanical charge distributions are almost identical and the slight difference is because of pure quantum effects like quantum beatings at the ends of the finite length nanotube (a cross check has been done with the use of periodic boundary conditions to exclude the finite length effects). Figure 8(a) shows typical charge density distributions calculated using the TBA and the Boltzmann equation for a cantilever SWNT of 50 nm long. We must conclude that a simple statistical description works fairly well for

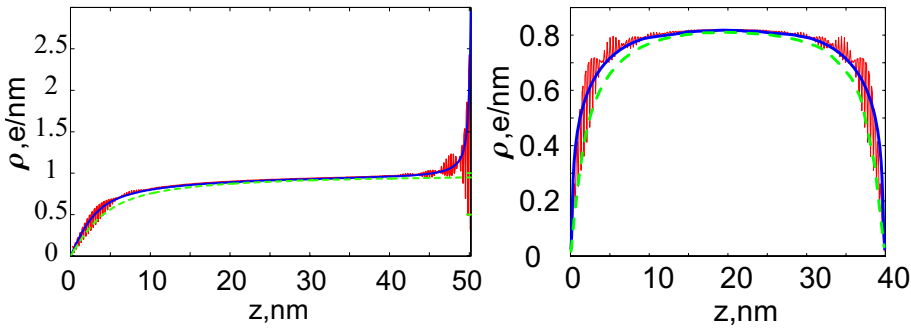


(a) (b)

Fig. 8. Specific charge density for two devices with geometry described in the text. The solid oscillating curve is a result of full quantum mechanical calculation. The solid line is a solution of joint Poisson and Boltzmann equations. The dotted line is our analytical approximation.

the case of straight ideal single-wall nanotube. Similar result is obtained for a string SWNT with two side contacts (Fig. 8(b)).

Thus, the analytical form of solution for the device electrostatics is a great simplification for calculating electrostatic forces in various NEMS devices, when a solution of a corresponding Poisson equation is known for a specific device geometry.

## 5. Conclusions

In summary, we present a continuum device theory for nanotube electromechanical systems. The theory gives a fast and accurate method for the simulation of charge density for a nanotube of an arbitrary shape displaced by a voltage applied to the nanotube end(s). The charge density is given by an atomistic capacitance of the nanotube. The atomistic capacitance is not defined solely by material properties of the nanotube itself. It depends also on the environment as the charge interaction in a low-dimensional electronic system of the nanotube is screened by the near-by placed electrodes.

We developed an analytical method to describe a nanotube NEMS and verified two main approximations used in the method: a model of an infinite wire for the geometric capacitance and a statistical model for the quantum capacitance. It is shown that the statistical approximation works fairly well, while the approximation of the infinite wire may lead to 6–7% error. Thus, the full electrostatics calculation has to be employed as described in this paper for obtaining the geometric capacitance, especially for nontrivial device geometries.

## Acknowledgments

Authors acknowledge support through a CRI grant of UIUC. S. V. Rotkin acknowledges DoE grant DE-FG02-01ER45932, and Beckman Fellowship from the Arnold

and Mabel Beckman Foundation. K. A. Bulashevich is grateful to Beckman Institute for hospitality during his work in Urbana.

## References

1. V. Derycke, R. Martel, J. Appenzeller, and Ph. Avouris, *Nano Lett.* **1**, 453 (2001); A. Bachtold, P. Hadley, T. Nakanishi, and C. Dekker, *Science* **294**, 1317 (2001).
2. S. Akita *et al.*, *Appl. Phys. Lett.* **79**(11), 1691 (2001).
3. E. Minot, V. Sazonova, Y. Yaish, J.-Y. Park, M. Brink, and P. McEuen, unpublished.
4. R. Saito, G. Dresselhaus, and M. S. Dresselhaus, *Physical Properties of Carbon Nanotubes* (Imperial College Press, London, 1998).
5. M. Dequesnes, S. V. Rotkin, and N. R. Aluru, *Nanotechnology* **13**, 120 (2002).
6. K. A. Bulashevich and S. V. Rotkin, *JETP Lett.* (Pis'ma v ZhETF) **75**(4), 205 (2002).
7. S. V. Rotkin, K. A. Bulashevich, and N. R. Aluru, in *Proceedings — Electrochemical Society*, eds. P. V. Kamat, D. M. Guldi, and K. M. Kadish (ECS Inc., Pennington, NJ, USA, 2002).
8. S. Luryi, *Appl. Phys. Lett.* **52**(6), 501 (1988).
9. L. D. Landau, E. M. Lifshitz, and L. P. Pitaevskii, *Electrodynamics of Continuous Media* (Pergamon, Oxford, UK, 1981).
10. J. H. Kane, *Boundary Element Analysis in Engineering Continuum Mechanics* (Prentice-Hall, 1994).
11. F. Shi, P. Ramesh, and S. Mukherjee, *Commun. Numer. Meth. Eng.* **11**, 691 (1995).
12. W. S. Hall, *The Boundary Element Method* (Kluwer Academic Publishers, 1994).